Eur. Phys. J. D **44**, 525–532 (2007)
DOI: 10.1140/epjd/e2007-00216-4

THE EUROPEAN PHYSICAL JOURNAL D

Fragmentation induced by charge exchange in collisions of charged alkaline clusters with alkali atoms

S. Díaz-Tendero[1], L.F. Ruiz[2], B. Zarour[3], F. Calvo[4], F. Spiegelman[4], P.-A. Hervieux[5], F. Martín[2], J. Hanssen[3], and M.F. Politis[1,a]

[1] Institut de Minéralogie et Physique des Milieux Condensés, Université Pierre et Marie Curie, Campus Boucicaut, 140 rue de Lourmel, 75015 Paris, France
[2] Departamento de Química, C-9, Universidad Autónoma de Madrid, 28049 Madrid, Spain
[3] Laboratoire de Physique Moléculaire et des Collisions, Institut J. Barriol (FR-CNRS 2843), Université de Metz, Technopôle 2000, 1 boulevard Arago, 57078 Metz Cedex 03, France
[4] Université Paul Sabatier, Laboratoire de Chimie et Physique Quantiques, UMR 5626, IRSAMC, 118 route de Narbonne, 31062 Toulouse, France
[5] Institut de Physique et Chimie des Matériaux de Strasbourg, GONLO, 23 rue Loess, 67034 Strasbourg, France

Received 16 March 2007
Published online 27 June 2007 –

Abstract. We present a theoretical study of the dissociative charge transfer processes induced by collisions between doubly-charged alkaline clusters and alkaline atoms at slow and intermediate impact energies. Charge-exchange cross sections have been evaluated for the collisions of Li_{31}^{2+} and Na_{31}^{2+} clusters with neutral alkaline atoms (Cs and Na) at impact energies between 500 and 4000 eV. The branching ratios of the evaporation processes have been calculated within the framework of the microcanonical statistical theory of Weisskopf. The key ingredient of this model is the cluster vibrational density of states. An approach based on quantum tight-binding Hamiltonian is introduced, allowing us to evaluate this quantity at a microscopic level, including quantum vibrational effects at low temperatures. Comparison with previously reported results obtained using a macroscopic description of the level density are presented and discussed.

PACS. 34.70.+e Charge transfer – 36.40.Qv Stability and fragmentation of clusters – 36.40.Wa Charged clusters

1 Introduction

Alkaline clusters are intermediate structures between atoms and solids, and therefore can be considered as atomic droplets. A large number of experimental and theoretical works have been carried out with the aim of understanding reactions involving electron excitation and fragmentation of those clusters [1–23]. In the particular case of cluster reactions involving electronic degrees of freedom, a collective response of the electrons can lead to the excitation of the cluster. The energy deposited in the cluster can be distributed among the vibrational modes leading to fragmentation (see e.g. [20]). In previous works we have studied charge transfer (CT) in collision of metal clusters and atoms and the subsequent fragmentation processes [20–22]. These studies have shown that in the experiments carried out with mass-selected clusters beams [3,5,17,19], the single CT of the valence electron ($6s$ for collisions with Cs and $3s$ for collisions with Na) is responsible for the production of small clusters through evaporation of atoms or dimers from the excited cluster [20–22].

In this work we present a theoretical study of evaporation of charged metal clusters induced by CT reactions in collisions with neutral atoms. In particular, we have studied collisions of the charged clusters Li_{31}^{2+} and Na_{31}^{2+} with the neutral alkaline atoms Cs and Na. Our study includes the evaluation of the CT cross sections and the subsequent fragmentation of the excited clusters:

$$Li_{31}^{2+} + Cs \rightarrow Li_{31}^{+} + Cs^{+} \rightarrow Li_{31-k}^{+} + Li_k + Cs^{+} \quad (1)$$

$$Li_{31}^{2+} + Na \rightarrow Li_{31}^{+} + Na^{+} \rightarrow Li_{31-k}^{+} + Li_k + Na^{+} \quad (2)$$

$$Na_{31}^{2+} + Cs \rightarrow Na_{31}^{+} + Cs^{+} \rightarrow Na_{31-k}^{+} + Na_k + Cs^{+}. \quad (3)$$

We compare the effect of different targets and different projectiles in a range of impact energies between 500 and 4000 eV. The theoretical framework we use to describe statistically the above reactions is based on the Weisskopf model, which requires the microcanonical densities of vibrational states (DOSs) as its key inputs. Unlike our previous efforts, where available thermodynamical data for the bulk metal provided estimates for the DOSs,

[a] e-mail: mpolitis@ccr.jussieu.fr

here we perform direct atomistic simulations of the specific cluster sizes using Monte Carlo methods and a quantum tight-binding Hamiltonian. This approach accounts for the possible nonmonotonic finite-size effects, which are not captured when simple scaling of the bulk data is used instead.

The objectives of this paper are (i) to compare charge transfer and fragmentation processes in collisions with different targets and different projectiles and (ii) to introduce a new methodology in the description of the density of states of the excited clusters to evaluate evaporation probabilities. The paper is organized as follows. In Section 2, we briefly present the theoretical methods employed. In Section 3 we present and discuss the results obtained. Comparison with the experimental measurements of Bréchignac et al. [21,22] is also given. The paper ends with the conclusions in Section 4. Atomic units are used throughout unless otherwise stated.

2 Theory

In the range of impact velocities considered in this work ($v \sim 0.01$–0.03 a.u. or 1–4 keV) the collision time ($\tau_{\rm col} \sim 10^{-14}$ s) is much shorter than the cluster vibrational period ($\tau_v \sim 10^{-12}$ s). Therefore, the only relevant degree of freedom during the collision is the relative distance between the cluster and the atom. In addition, the electron-phonon coupling, which is responsible for the cluster fragmentation, has a characteristic lifetime of $\tau_{\rm rel} \sim 10^{-13}$–$10^{-12}$ s. Thus, the electronic excitation energy deposited during the collision will be relaxed into vibrational degrees of freedom well after the collision, leading to the fragmentation of the cluster. In summary, the different time scales of the processes taking place in these reactions allow us to evaluate the fragmentation separately from the collision, i.e. as a post-collisional process, the energy deposited in the collision being the quantity that relates both processes.

In this section we present the theoretical methods employed for the evaluation of the collision dynamics, the charge transfer cross sections, the energy deposit and the fragmentation of the excited clusters.

2.1 Collision dynamics

For the description of the alkaline atom we suppose that the valence electron is the only active electron and the others together with the nuclei form a frozen core. We describe the interaction of the electron with the frozen core by means of a model potential technique in which the electron moves in a spherical potential [24]. Moreover, the main simplifying assumption in our simulations is the complete neglect of ionic geometry through the use of the spherical jellium model. This model consists in replacing the actual potential of the underlying ionic frame by the potential of a sphere of radius R_C with a constant and uniform positive charge distribution [7,16]. This is a reasonable approximation [25] for the description of large electronic alkaline clusters and, especially if the cluster is hot and disordered ($T \sim 500$ K): in such states the cluster fluctuates between many disordered isomers, and is definitely not frozen in its lowest-energy geometry. The liquid state of the cluster is further confirmed by the caloric curves, shown and discussed below in Figure 2 and previously calculated in references [26,27] for sodium case. Thus, in this range of temperatures and internal energies, the spherical jellium approximation provides, on average, a more realistic picture of the cluster than that corresponding to the lowest-energy geometry. Only at very low temperatures, specific size effects on the electronic structure are expected to play some role (if any).

We have then followed the methodology presented in reference [7] for the description of the N_e valence electrons of the cluster ($N_e = 29$ for Li_{31}^{2+} and Na_{31}^{2+}). It consists in applying the Kohn-Sham formulation of the density-functional theory to describe the electronic density of the cluster in terms of single-particle orbitals. From these orbitals we obtain the corresponding one-electron potentials using the local-density approximation with exchange, correlation and self-interaction correction (LDAXC-SIC). The orbital-dependent potentials obtained with this method exhibit the correct asymptotic Coulombic behavior, which is crucial in this work because CT and excitation occur mainly at large distances. We have used in our simulations a global average potential from the calculated orbital-dependent LDAXC-SIC potential. The orbitals and the potentials are then used in the dynamical simulations of the collision. In particular, the molecular approach for ion-atom collisional problems at low energies has been used. In collisions where many electrons are active, this approximation enables us to describe multi-electronic processes such as transfer-excitation or multi-excitation of the projectile. The N_e-body problem was solved within the independent electron model (IEM) and the inclusive probability method introduced by Lüdde and Dreizler [28]. A full quantum-mechanical description in the IEM is possible because each active electron moves in the field produced by two potentials: the model potential for the target and the LDAXC-SIC potential of the cluster. Thus, the total Hamiltonian $\widehat{H}$ can be expressed as a sum of N_e one-electron effective Hamiltonians:

$$\widehat{H} \cong \sum_{j=1}^{N_e} \widehat{h}_j. \tag{4}$$

For each j in the above expression we have:

$$\widehat{h}_j \equiv \widehat{h} = -\frac{1}{2}\nabla^2 + V_{\rm A^+}(|\boldsymbol{r}\text{-}\boldsymbol{R}|) + V_{\rm C}(\boldsymbol{r}), \tag{5}$$

where, $V_{\rm A^+}$ is the model potential of Cs^+ or Na^+ [24] and $V_{\rm C}$ the cluster common average LDAXC-SIC potential [20,22]. As the cluster mass is much larger than the target mass, the electronic coordinates have been put on the cluster center of mass, $\boldsymbol{R}$ being the position vector of the target nucleus and $\boldsymbol{r}$ that of the valence electron. The dynamical problem associated to the one-electron Hamiltonian $\widehat{h}$ is solved in the semi-classical approach

where the projectile is treated classically in the impact-parameter formalism and the electron motion is described quantum mechanically. Thus, for each orbital j, one has to solve the time dependent Schrödinger equation:

$$\widehat{h}\Psi_j(\boldsymbol{r},t) = i\frac{d}{dt}\Psi_j(\boldsymbol{r},t),\ j = 1,\ldots,N_e, \tag{6}$$

with the initial conditions:

$$\lim_{t\to-\infty}\Psi_j(\boldsymbol{r},t) = \phi_j(\boldsymbol{r})\exp[-i\epsilon_j t], \tag{7}$$

where $\phi_j(\boldsymbol{r})$ is the initial ($t = -\infty$) spin-orbital of energy ϵ_j.

In the experimental studies and in the range of impact energies covered by the present work, the collision velocities are always smaller than the velocity of one electron in any jth orbital. This fact justifies the use of the molecular approximation for the description of the ion-atom (cluster-atom) collision. Equation (5) is solved by expanding the wave function $\Psi_j(\boldsymbol{r},t)$ on a basis of Born-Oppenheimer (BO) molecular states $\{\chi_k(\boldsymbol{r},\boldsymbol{R})\}$. These molecular states have been obtained by diagonalizing $\widehat{h}$ in a two-center atomic basis built from spherical Gaussian-type orbitals (GTOs) with angular momentum $\ell \leq 6$.

2.2 Charge transfer cross section

Charge transfer cross sections have been evaluated using the inclusive probability method [28], which consists in calculating the quantity $P_{f_1\cdots f_q}$ of finding q of the N_e electrons in the sub-configuration $(f_1\cdots f_q)$ while the remaining $N_e - q$ electrons occupy any other states after the collision. This probability is given by the $(q\times q)$ determinant [28]:

$$P_{f_1\cdots f_q} = \det(\gamma_{nn'});\quad n,n' = 1,\ldots,q;\ q < N_e, \tag{8}$$

where $\gamma_{nn'}$ is the one-particle density matrix. The inclusive probability of finding q occupancies and $L-q$ holes, $P^{f_{q+1}\cdots f_L}_{f_1\ldots f_q}$, can be written in terms of the probabilities (8) related only to occupancies [28]. We have successfully used this procedure in previous works [7,16,23]. In order to determine the charge transfer cross section $\sigma_{\rm CT}$ we must evaluate for each impact parameter b the following inclusive probabilities:

$$P^{6s,\overline{6s},6p,\overline{6p}\ldots}\quad\text{and}\quad P_j^{6s,\overline{6s},6p,\overline{6p}\ldots}\ \text{for Cs}, \tag{9}$$

and

$$P^{3s,\overline{3s},3p,\overline{3p}\ldots}\quad\text{and}\quad P_j^{3s,\overline{3s},3p,\overline{3p}\ldots}\ \text{for Na}, \tag{10}$$

where $n\ell$ and $\overline{n\ell}$ are the orbitals with the corresponding α and β spin components, respectively. Equations (9) and (10) represent the probabilities of finding no electrons in the atomic valence orbitals ($6s, 6p,\ldots$ for Cs and $3s, 3p,\ldots$ for Na) and the probability that, simultaneously, an electron is found in the j initially unoccupied orbital of the cluster (both for Li_{31}^{2+} and Na_{31}^{2+}, $j = 2p, 1g, 3s, 2d, 1h, 3p, 2f, 4s, 3d,\ldots$).

Finally, the CT cross section has been evaluated by integration of the corresponding probability over the impact parameter:

$$\sigma_{\rm CT} = \int_{R_{\rm C}}^{\infty} bP_{\rm CT}(b)\mathrm{d}b \tag{11}$$

where $P_{\rm CT} = P^{6s,\overline{6s},6p,\overline{6p},\ldots}$ for Cs and $P_{\rm CT} = P^{3s,\overline{3s},3p,\overline{3p},\ldots}$ for Na.

2.3 Energy deposit

As already pointed out, the quantity that relates the collision with the fragmentation is the energy deposited in the cluster during the CT process. Labelling Li_{31} and Na_{31} as M_N, with M = Li or Na and $N = 31$, the total internal excitation energy in the cluster after the collision is given by:

$$E^*_{M_N^+}(b) = E_0^* + \delta E_{M_N^+}(b), \tag{12}$$

where E_0^* is the initial vibrational energy of the M_N^{2+} cluster before the collision and $\delta E_{M_N^+}(b)$ its electronic excitation energy due to CT, i.e. the energy deposited in the collision. In our model [22], $\delta E_{M_N^+}$ is given by:

$$\delta E_{M_N^+}(b) = \sum_j \Delta\epsilon_j P_j^{ns,\overline{ns},np,\overline{np}\ldots}(b), \tag{13}$$

where $\Delta\epsilon_j = \epsilon_j - \epsilon_{1f}$. ϵ_j and ϵ_{1f} are the electron energy in an excited j orbital and in the last initially occupied cluster orbital $1f$, respectively. In equation (13), $n = 6$ for Cs and $n = 3$ for Na.

The total excitation energies calculated with the previous formulae are then used to evaluate the fragmentation rates as explained in the next section. Therefore, the internal energy after the collision is the relevant quantity that will determine the fragmentation behavior.

2.4 Fragmentation of excited clusters

After the collision, the main dissociation channel of the excited clusters is the sequential evaporation of monomers or dimers [3,20,22]. Following [22], the evaporation rates for a monomer $k_{N,1}$ and for a dimer $k_{N,2}$ were evaluated in the framework of the microscopic, microcanonical statistical model of Weisskopf [29]. These rates depend on the vibrational density of states $\rho_N^v(E_N^*)$, which is a function of the internal excitation energy $[E_N^* \equiv E^*_{M_N^+}]$. $\rho_N^v(E_N^*)$ has been determined via the specific entropy $s(\epsilon)$ and internal energy $\epsilon(T)$ per atom, respectively given by

$$\epsilon(T) = \int_0^T c_v(T')dT', \tag{14}$$

$$s(\epsilon) = \int_0^T \frac{c_v(T')}{T'}dT', \tag{15}$$

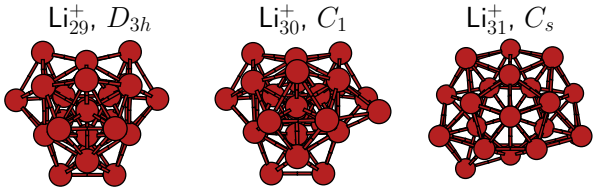

Fig. 1. Most stable isomers of Li_{29}^+, Li_{30}^+ and Li_{31}^+.

where $c_v(T)$ is the specific heat at constant volume and temperature T. In the microcanonical ensemble, the entropy $S_N(E_N^*) = Ns(\epsilon)$ is related to the level density by the well-known formula:

$$k_B \ln[\rho_N^v(E_N^*)] = Ns(\epsilon). \tag{16}$$

The calculation of the specific heat was carried out following the methodology introduced in reference [30]. In this method, the binding energy of the lithium clusters is modelled using a version of the quantum tight-binding (TB) Hamiltonian previously developed for sodium clusters [30], and further adapted for silver clusters [31]. Using the notations of reference [30], the distance-dependent hopping integrals $t_{ss}(r)$ and $t_{sz}(r)$ are both taken as $t(r) = Ar^p \exp(-ar)$. The diagonal interaction $\varrho(r)$ accounts for the short-range repulsion as well as an effective long-range dispersion attraction:

$$\varrho(r) = B\exp(-br) - f_{\rm cut}(r)\frac{C}{r^\nu}, \tag{17}$$

with a cut-off function $f_{\rm cut}$ taken as an Aziz form [32] and with a cut-off radius d. All parameters were numerically obtained by fitting the potential curves of the two lowest electronic states of Li_2 and the dissociation energy of Li_4. They are given by $A_{ss} = -1.95 \times 10^{-4}$ and $A_{sz} = 9.1\times10^{-6}$ Hartree; $p_{ss} = 8$ and $p_{sz} = 10$; $a_{ss} = 1.80$ and $a_{sz} = 1.65$ bohr^{-1} for the hopping integrals, and by $B = 2.406$ Hartree, $b = 1.494$ bohr^{-1}, $C = 6.587$ a.u., $\nu = 5.90$, and $d = 4.826$ bohr for the diagonal term. We first performed a global survey of the potential energy surfaces (PESs) of the three clusters Li_N^+ at $N = 29$, 30, 31, by locally optimizing a set of candidate structures obtained previously for metal clusters, using a similar strategy as the one in reference [33] for cationic sodium clusters. The classical caloric curves were computed using canonical Monte Carlo (MC) simulations improved with the parallel tempering strategy [34]. 57 replicas were chosen with a geometric allocation of temperatures in the range 5 K $\leq T \leq$ 1500 K. The simulations consisted of 10^6 MC cycles, following 2×10^5 steps left out for equilibration. The clusters were confined in a sphere of radius 12 bohr to prevent evaporation. Configuration exchanges between adjacent trajectories were attempted with 10% probability. Because parallel tempering also stands as a structural optimization method, we could further refine the putative global minima found previously. The most stable isomers obtained using this combination of methods are depicted in Figure 1. They are all based on icosahedra, with an anti-Mackay (or polyicosahedral) overlayer, similar to the geometries found for rare-gas clusters. Due to the light weight of the lithium element, the dynamics and thermodynamics of lithium clusters can be sensitive to vibrational quantum delocalization. We have used the Pitzer-Gwinn (PG) approximation [35] to correct for the low-temperature variations in the caloric curve. Briefly, the PG approach consists in approximating the anharmonic quantum partition function $Z_{\rm q}$ at temperature T by the product of the anharmonic classical partition function and the ratio of the quantum to classical partition functions of the harmonic system:

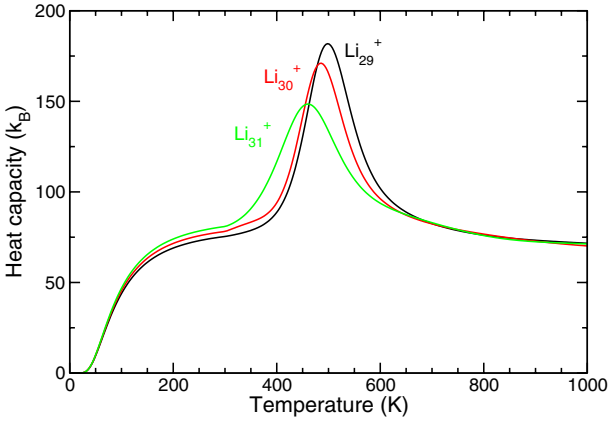

Fig. 2. (Color online) Heat capacities of Li_{29}^+, Li_{30}^+ and Li_{31}^+ obtained from classical parallel tempering Monte Carlo simulations corrected for vibrational quantum effects using the Pitzer-Gwinn approximation.

$$Z_{\rm q}(T) \approx Z_{\rm c}(T)\frac{Z_{\rm q}^{\rm H}(T)}{Z_{\rm c}^{\rm H}(T)}. \tag{18}$$

The harmonic partition functions are taken for the global minima, which are characterized by a set of vibrational frequencies $\{\omega_i\}$:

$$\frac{Z_{\rm q}^{\rm H}(T)}{Z_{\rm c}^{\rm H}(T)} = \prod \frac{\sinh \hbar\omega_i/k_{\rm B}T}{\hbar\omega_i/k_{\rm B}T}, \tag{19}$$

where $k_{\rm B}$ and $\hbar$ are the Boltzmann constant and the Planck constant, respectively. While these quantum corrections are most sensitive at low temperatures, it should be noticed that they could affect the global minimum itself. With the inclusion of zero-point energy contributions, the ordering between isomers may change and a new quantum global minimum may appear [36]. However, in the present case, the anti-Mackay character of the global minima of the clusters makes this situation unlikely, as the anti-Mackay structures are usually further stabilized by zero-point effects [36].

The quantum-corrected heat capacities of the three clusters (Li_{31}^+, Li_{30}^+ and Li_{29}^+) are represented in Figure 2. Each curve exhibits three distinct regions. At low temperature, the heat capacity increases from zero to a plateau close to the Dulong-Petit limit $(3N - 6)k_{\rm B}$, then reaches a peak characteristic of the solidlike-liquidlike transition, and finally decreases down to a second plateau. Quantum

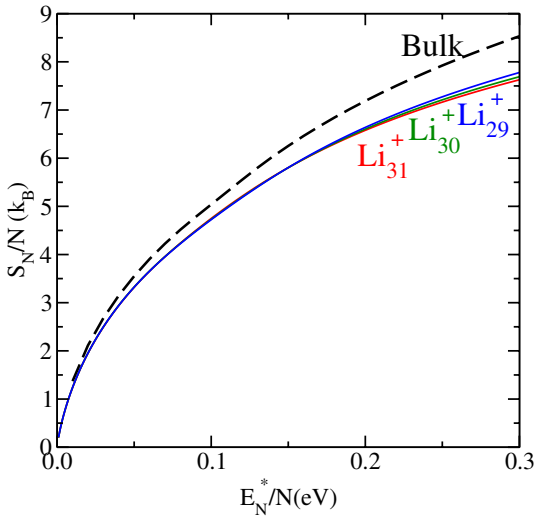

Fig. 3. (Color online) Specific entropy as a function of the internal energy per atom for Li_{31}^+, Li_{30}^+, Li_{29}^+ (full lines) and bulk lithium (dashed line).

corrections are mostly important in the low temperature range $0 \leq T \leq 200$ K, where the heat capacity lies significantly below $(3N-6)k_B$. The melting temperature T_{melt} is indicated by the top of the peak, and the latent heat of fusion is the area below the peak. T_{melt} varies decreasingly with increasing size: 500 K for the smallest cluster, 485 K for Li_{30}^+, and only 460 K for Li_{31}^+. These values are comparable to the bulk melting temperature (about 454 K). For clusters they are probably overestimated, due to our TB model being fitted on molecular properties without including proper bulk data [26]. However, as will be seen below, this barely affects the evaporation rates, which are essentially sensitive to the sharper variations of the densities of states. That both the melting temperature and the latent heat vary decreasingly is a manifestation of non-monotonic size effects, as experimentally demonstrated by the Haberland group [37].

The variation of the entropy as a function of the internal energy E_N^* as given by equations (14–16) is shown in Figure 3. In the same figure the entropy of bulk lithium is also shown [22]. We observe that the entropy given by the bulk approximation compares fairly well with our microscopic calculations in the region of energies lower than 0.15 eV/N, which is approximately (as will be shown below) the total excitation energy of the cluster. Moreover, the difference between the calculated entropies for the Li_N^+ clusters ($N = 29$, 30 and 31) in this region is almost negligible. For the evaporation simulations we have used both the bulk and the calculated finite-size entropies in order to obtain the densities of states and from them, the monomer and dimer fragmentation rates (see [20] for the complete equations):

$$k_{N,1} \propto \int \frac{\rho_{N-1}^v}{\rho_N^v} e\, de \propto \int \frac{\exp(S_{N-1}/k_B)}{\exp(S_N/k_B)} e\, de \quad (20)$$

$$k_{N,2} \propto \int \frac{\rho_{N-2}^v}{\rho_N^v} e\, de \propto \int \frac{\exp(S_{N-2}/k_B)}{\exp(S_N/k_B)} e\, de. \quad (21)$$

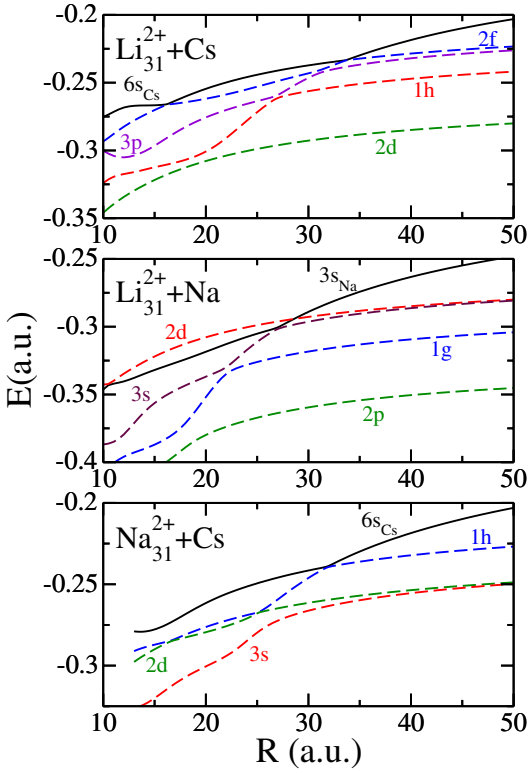

Fig. 4. (Color online) Correlation diagrams (energy versus cluster-atom distance R) for the σ molecular orbitals of $(Li_{31}{-}Cs)^{2+}$ (upper panel), $(Li_{31}{-}Na)^{2+}$ (middle panel) and $(Na_{31}{-}Cs)^{2+}$ (lower panel). $n\ell$, $6s_{Cs}$ and $3s_{Na}$ denote, respectively, the cluster, Cs and Na orbitals to which the MOs correlate at $R = +\infty$.

Although the difference in entropy per atom is small, the fragmentation ratio scales as the exponential of the difference between the entropy of the parent and the daughter clusters (s_N, s_{N-1} or s_{N-2}), as can be seen in the above equations. Thus, small differences in entropy per atom could lead to great differences in the evaporation rates. The rates ($k_{N,1}$ and $k_{N,2}$) are then introduced in a set of coupled master equations (which are integrated up to the time of flight of the experiment we want to compare with). We thus obtain the branching ratios for the production of Li_N^+ or Na_N^+ clusters with sizes $N = 31, 30, 29, \ldots$ The results obtained with both approximations are presented in the next section.

3 Results and discussions

Figure 4 shows the adiabatic BO energy correlation diagrams for the three systems studied and for the $\sigma(m = 0)$ molecular orbitals. These orbitals have been obtained by diagonalizing $\widehat{h}$ in a two-centre *atomic* basis built from spherical Gaussian-type orbitals (GTO) with angular momentum up to $l = 6$. The orbital energies in the figure are labelled from their analogues at $R = +\infty$ ('separate atom') and therefore, the initially occupied orbitals are: $1s, 1p, 1d, 2s$ and $1f$ for the clusters, $6s$ for the Cs and $3s$

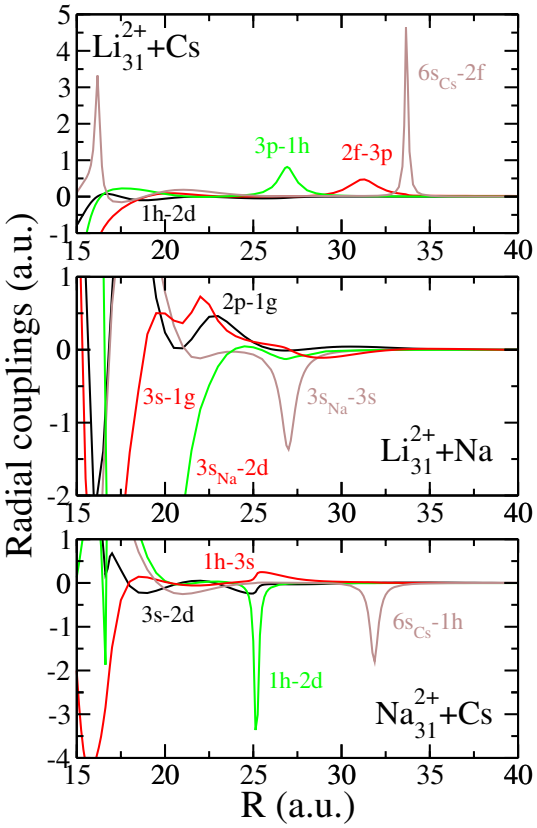

Fig. 5. (Color online) Non adiabatic radial couplings between the σ molecular orbitals of $(Li_{31}-Cs)^{2+}$ (upper panel), $(Li_{31}-Na)^{2+}$ (middle panel) and $(Na_{31}-Cs)^{2+}$ (lower panel) versus cluster-atom distance R. $n\ell$, $6s_{Cs}$ and $3s_{Na}$ denote, respectively, the cluster, Cs and Na orbitals to which the MOs correlate at $R = +\infty$.

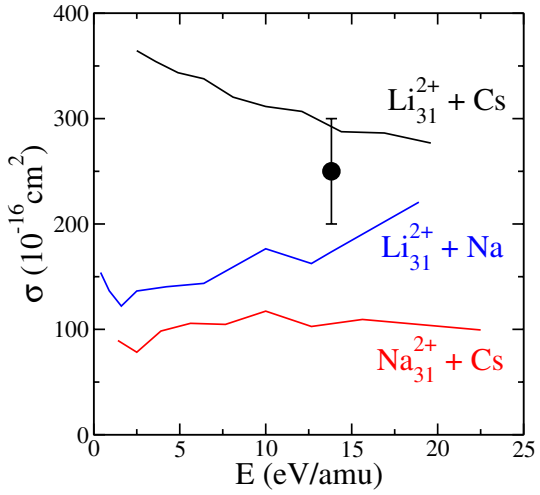

Fig. 6. (Color online) Total cross sections (σ_{CT}) versus impact energy for $(Li_{31}–Cs)^{2+}$, $(Li_{31}–Na)^{2+}$ and $(Na_{31}–Cs)^{2+}$. The experimental measurement of Bréchignac et al. [22] for the Li_{31}^{2+}+Na is given by the symbol with error bar.

for the Na. Figure 5 shows the relevant non adiabatic radial couplings between the one-electron states of Figure 4. A first inspection of the correlation diagrams and the radial couplings shows that the effective avoided crossings are located at large distances. More precisely, the upper panels of Figures 4 and 5 show that the entrance channel [Cs($6s$)] is mainly coupled with the empty cluster orbitals $2f$, $3p$, $1h$ and $2d$ with the effective avoided crossings placed at $R \sim 20$–35 a.u. The middle panels of Figures 4 and 5 show that the entrance channel [Na($3s$)] is coupled with the $2d$, $3s$, $1g$ and $2p$ cluster orbitals. The lower panels of Figures 4 and 5 show that the input channel [Cs($6s$)] is coupled with the $1h$, $2d$ and $3s$ cluster orbitals and the important avoided crossings take place at $R \sim 25$–35 a.u. Thus, in all cases, the CT process is expected to take place at large distances ($R \sim 20$–35 a.u).

Figure 6 shows the total charge transfer cross section σ_{CT} as a function of the impact energy for the three systems under study. The shape of the cross sections varies with the collisional system: while it slightly increases with the impact energy in the Li_{31}^{2+}+Na collision, it decreases in the Li_{31}^{2+}+Cs one and remains practically constant in the Na_{31}^{2+}+Cs case. We can also see that the CT cross section for the Li_{31}^{2+}+Cs collision is larger than the one for the Li_{31}^{2+}+Na collision. In the Na_{31}^{2+}+Cs collision, σ_{CT} is the smallest of the three systems in the range of impact energies studied. These results can be understood by analyzing the correlation diagrams depicted in Figures 4 and 5. For the collision of Li_{31}^{2+} with Cs, the effective avoided crossings are located at larger distances than in the case of Li_{31}^{2+} with Na. Therefore, CT occurs at larger distances and the corresponding cross section is necessarily larger. This is so in spite of the fact that the avoided crossing at $R \sim 34$ a.u. is passed through diabatically (because the corresponding radial coupling has a narrow Lorentzian shape in that region and contains an area of $\pi/2$ [38,39], see Fig. 5) and the first effective avoided crossing is that appearing at $R \sim 31$ a.u. For Na_{31}^{2+}+Cs, the avoided crossing appearing at around $R \sim 35$ a.u. is passed through diabatically. As a consequence, the first effective avoided crossings appear at smaller distances ($R \sim 25$ a.u.), thus leading to smaller cross sections. In Figure 6 we have also represented the experimental measurements of Bréchignac et al. [22] for the Li_{31}^{2+}+Cs system at an impact energy of 3 keV (∼14 eV/amu). The comparison between theory and experiment is very satisfactory.

The left column of Figure 7 shows the calculated energy deposited in the three collisions [see Eq. (13)] as a function of the impact parameter $\delta E_{M_N^+}(b)$ (solid line) and its average value $\left\langle \delta E^*_{M_N^+} \right\rangle$ (horizontal dashed line) for a collision velocity of $v_{col} \sim 0.023$–0.025 a.u. The oscillations observed in the energy deposit are due to the oscillatory behavior of the transition probabilities (see e.g. Ref. [22] for the Li_{31}^{2+}+Cs case). We note that the average value depends on the collisional system (varying between ∼0.5 and 2.0 eV). This effect can be also understood from the correlation diagrams (Fig. 4). For example, it can be seen that the largest value of R at which the energy is efficiently deposited coincides with the position of the

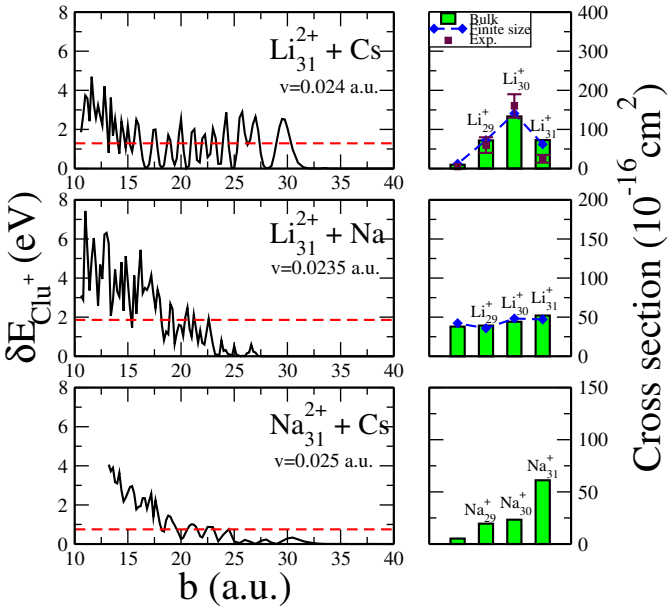

Fig. 7. (Color online) (Left panels) Energy deposit as a function of the impact parameter for $(Li_{31}–Cs)^{2+}$, $(Li_{31}–Na)^{2+}$ and $(Na_{31}–Cs)^{2+}$. The horizontal dashed line represents the average value $\left\langle \delta E_{M_N^+} \right\rangle$. (Right panels) Partial cross sections of M_N^+ cluster production with $N = 31$, 30, 29 and all $N < 29$, M = Li or Na. The symbols with error bars are experimental data given in [22].

farthest efficient avoided crossing (see also the discussion of the previous paragraph).

We have previously shown that for a correct interpretation of the experiment of Bréchignac et al. two parameters play a crucial role [21,22]: (i) the time-of-flight (TOF) at which the fragments are detected and (ii) the initial vibrational energy (E_0^*) of the clusters before the collision. In order to have a direct comparison with these experiments we have taken a TOF of 3 μs and an initial cluster energy of $E_0^* = 4.1$ eV in the three systems studied.

In the right side of Figure 7 (upper and middle panels) the partial cross sections for the production of Li_{31}^+, Li_{30}^+, Li_{29}^+ and $\sum Li_N^+$ (with $N < 29$) are shown. For the Li_{31}^{2+}+Cs collision, the partial cross sections evaluated with both methods (bulk entropy and calculated finite size entropy) are in good agreement with the experimental data [22] being the finite-size ones the nearest to the experimental ones. For the Li_{31}^{2+}+Na collision, the cross sections obtained by using the bulk and the finite-size entropy are practically the same. For the first collisional system, the Li_{30}^+ fragment is greatly dominant in comparison with Li_{31}^+, Li_{29}^+ and smaller fragments. On the other hand, in the Li_{31}^{2+}+Na collision the partial cross sections are all equivalent in magnitude ($\sim 50 \times 10^{-16}$ cm^2). Indeed, $\left\langle \delta E_{Clu_N^+} \right\rangle$ for the Li_{31}^{2+}+Na collision is almost twice as large as for the Li_{31}^{2+}+Cs case, which leads to a larger production of smaller fragments. On the other hand, for the Na_{31}^{2+}+Cs collision, $\left\langle \delta E_{M_N^+} \right\rangle$ is the smallest of the three collisional systems and, therefore, the lowest evaporation is observed, the fragment Na_{31}^+ being the dominant species. Only the bulk entropy of Na was used in this case [20].

4 Conclusion

We have presented a theoretical study of charge transfer and evaporation in collisions of slow metallic clusters (Li_{31}^{2+} and Na_{31}^{2+}) with alkali atoms (Cs and Na). The calculated charge transfer is in reasonable agreement with the available experimental cross section. We have shown that the entropy determined either by a bulk model or by a finite size model are very similar in the range of energies we are interested in. Therefore no noticeable variations in the fragmentation rates are obtained, which leads to very similar evaporation results. In any case, the fragmentation results obtained with the finite-size entropy are in slightly better agreement with the experimental data. In addition to the crucial role played by the TOF and the initial energy of the cluster, we have shown that evaporation strongly depends on how the cluster excited states are populated during the collision. This is clearly illustrated by comparing the collision energy deposit and the resulting fragmentation branching ratios for the three systems. As expected, we observe a larger distribution of fragments when the energy deposited during the collision is high.

We thank the CCC-UAM for allocation of computer time. Work partially supported by the DGI (Spain), project Nos. FIS2006-00298 and CTQ2004-00039/BQU.S. D-T. acknowledges the support of the HPC-EUROPA program, funded under the European Commission's Research Infrastructures activity, contract number RII3-CT-2003-506079.

References

1. J. Perel, H.L. Daley, *Electronic and Atomic Collisions*, edited by B.C. Cobic, M.V. Kurepa (Beograd, Yugoslavia, 1973), Vol II
2. C. Klots, J. Chem. Phys. **83**, 5854 (1985); C. Klots, Z. Phys. D **5**, 83 (1987)
3. C. Bréchignac, Ph. Cahuzac, J. Leygnier, R. Pflaum, J. Weiner, Phys. Rev. Lett. **61**, 314 (1988)
4. C. Bréchignac, Ph. Cahuzac, J. Leygnier, J. Weiner, J. Chem. Phys. **101**, 6992 (1994)
5. C. Bréchignac, Ph. Cahuzac, F. Carlier, M. Frutos, Phys. Rev. B **49**, 2825 (1994)
6. F. Martín, P.A. Hervieux, J. Hanssen, M.E. Madjet, M.F. Politis, Phys. Rev. B **58**, 6752 (1998)
7. M.F. Politis, P.A. Hervieux, J. Hanssen, M.E. Madjet, F. Martín, Phys. Rev. A **58**, 367 (1998)
8. U. Saalmann, R. Schmidt, Phys. Rev. Lett. **80**, 3213 (1998)
9. O. Knospe, J. Jellinek, U. Saalmann, R. Schmidt, Eur. Phys. J. D **5**, 1 (1999)
10. F. Martín, M.F. Politis, B. Zarour, P.-A. Hervieux, J. Hanssen, M.E. Madjet, Phys. Rev. A **60**, 4701 (1999)
11. F. Martín, M.E. Madjet, P.A. Hervieux, J. Hanssen, M.F. Politis, R.S. Berry, J. Chem. Phys. **111**, 8934 (1999)

12. D. Babikov, E.A. Gislason, M. Sizun, F. Aguillon, V. Sidis, J. Chem. Phys. **112**, 7032 (2000); M. Guissani, V. Sidis, J. Chem. Phys. **102**, 1288 (1995); M. Guissani, V. Sidis, Z. Phys. D **40**, 221 (1997)
13. C. Bréchignac, Ph. Cahuzac, B. Concina, J. Leygnier, I. Tignères, Eur. Phys. J. D **12**, 185 (2000)
14. F. Calvayrac, P.-G. Reinhard, E. Suraud, C.A. Ullrich, Phys. Rep. **337**, 493 (2000)
15. O. Knospe, J. Jellinek, U. Saalmann, R. Schmidt, Phys. Rev. A **61**, 022715 (2000)
16. B. Zarour, J. Hanssen, P.A. Hervieux, M.F. Politis, F. Martín, J. Phys. B **33**, L707 (2000)
17. M. Barat, J.C. Brenot, H. Dunet, J.A. Fayeton, Y.J. Picard, J. Chem. Phys. **114**, 179 (2001)
18. P. Blaise, S.A. Blundell, C. Guet, R.R. Zope, Phys. Rev. Lett. **87**, 063401 (2001)
19. C. Bréchignac, Ph. Cahuzac, B. Concina, J. Leygnier, Eur. Phys. J. D **16**, 91 (2001)
20. P.A. Hervieux, B. Zarour, J. Hanssen, M.F. Politis, F. Martín, J. Phys. B **34**, 3331 (2001)
21. C. Bréchignac, Ph. Cahuzac, B. Concina, J. Leygnier, L.F. Ruiz, B. Zarour, P.A. Hervieux, J. Hanssen, M.F. Politis, F. Martín, Phys. Rev. Lett. **89**, 183402 (2002)
22. C. Bréchignac, Ph. Cahuzac, B. Concina, J. Leygnier, L.F. Ruiz, B. Zarour, P.A. Hervieux, J. Hanssen, M.F. Politis, F. Martín, Phys. Rev. A **68**, 063202 (2003)
23. P.A. Hervieux, L.F. Ruiz, S. Diaz-Tendero, M. Alcami, B. Zarour, M.F. Politis, J. Hanssen, F. Martín, Phys. Scripta **T110**, 308 (2004)
24. H. Bachau, Ph. Galan, F. Martín, Phys. Rev. A **41**, 3534 (1990)
25. M. Brack, Rev. Mod. Phys. **65**, 67 (1993)
26. F. Calvo, F. Spiegelmann, J. Chem. Phys. **112**, 2888 (2000)
27. F. Calvo, F. Spiegelmann, Phys. Rev. Lett. **89**, 266401 (2002)
28. H. Lüdde, R.M. Dreizler, J. Phys. B **18**, 107 (1985)
29. V. Weisskopf, Phys. Rev. **52**, 295 (1937)
30. R. Poteau, F. Spiegelmann, Phys. Rev. B **45**, 1878 (1991); J. Chem. Phys. **98**, 6540 (1993)
31. R. Poteau, J.-L. Heully, F. Spiegelmann, Z. Phys. D **40**, 479 (1997)
32. R.A. Aziz, H.H. Chen, J. Chem. Phys. **67**, 5719 (1977)
33. F. Calvo, S. Tran, S.A. Blundell, C. Guet, F. Spiegelmann, Phys. Rev. B. **62**, 10394 (2000)
34. G.J. Geyer, in *Computing Science and Statistics: Proceedings of the 23rd Symposium on the Interface*, edited by E.K. Keramidas (Interface Foundation, Fairfax Station, 1991), p. 156
35. K.S. Pitzer, W.D. Gwinn, J. Chem. Phys. **10**, 428 (1942)
36. F. Calvo, J.P.K. Doye, D.J. Wales, J. Chem. Phys. **114**, 7132 (2001)
37. M. Schmidt, R. Kusche, B. von Issendorff, H. Haberland, Nature **393**, 238 (1998)
38. C. Zener, Proc. R. Soc. Lond. A **137**, 696 (1932)
39. L.D. Landau, Phys. Z **2**, 46 (1932)